Response of Integral Armor Under High Velocity Impact An Experimental and Finite Element Study

Hassan Mahfuz, Yuehui Zhu, Anwarul Haque,
Uday Vaidya and Shaik Jeelani
Tuskegee University's Center for Advanced Materials (T-CAM)
Tuskegee University, Tuskegee, Alabama 36077

SUMMARY :

Finite element analysis using LS-DYNA3D has been performed to investigate the response of an integral armor under high velocity impact. The analysis is based on actual experiments conducted in a gas gun set up. A 3-D model consisting of the various discrete layers of the armor has been developed and subjected to transient dynamic loading. The geometry and boundary conditions are all pertinent to the experiment. The projectile is blunt ended and is made from a hardened 4340 steel rod. The integral armor is a 300 mm x 300 mm x 46mm plate with multi-component layers of AD-90 ceramic, EPDM rubber, S2-glass/Vinyl ester and phenolic composites. V_{50} velocity for a fragment simulated projectile (FSP) has been considered, and the corresponding responses have been investigated to assess the failure of the armor at the ballistic limit. The analyses also provided information regarding the extent of the damage zone in the neighborhood of the bullet. The correlation with the experimentally observed damage zone was in good agreement with the FE analysis. Stress distributions through the thickness has been determined and the maximum value was found to occur at the ceramic layer. From the delamination point of view the two interfaces across the rubber layer were found to be most critical. Interlaminar tensile and shear stress distributions have also been examined, and their contributions to the failure of the armor are discussed.

KEYWORDS : Composite structures, impact, finite element method (FEM)

Introduction:

Ever since the discovery in the sixties that ceramic backed by glass reinforced plastics provide an excellent weight efficient armor system for arresting the high velocity projectiles, the development of the multi-layered integral armor has progressed in a hectic pace. Extensive use of fibers and reinforced plastics as armor and shielding components can be found in defense as well as in commercial applications. Recent introduction of Kevlar and S2-glass fibers in armor systems further enhanced their performances in ballistics and structural fronts. Today's integral armor is not only expected to stop the piercing bullet but also to support and endure significant structural loads. Over the years the structural composition of the integral armor has changed significantly. In order to increase the combat efficiency of the vehicle signature layer made of reinforced composites has been added at the outermost layer to increase the stealth characteristics. To improve the safety of the personnel, composite layer made from phenolics has been incorporated in the armor to enhance the fire, smoke and toxicity (FST) characteristics. A rubber layer between the ceramic and structural composites has been introduced to absorb the impact energy through viscous damping and to add multi-hit capability to the armor.

The ceramic is not any more continuous but consisted of adhesively bonded multiple hexagonal tiles which help contain the ballistic damages within minimum number of tiles. Bonded tiles also make the armor suitable for repair. It is therefore, evident that the complexity of the armor construction has increased many folds and so did its structural analysis.

Since the target, in this case the armor, is composed of various materials systems, stress pulses incident to an interface will have components transmitted and reflected waves depending on the mechanical impedance, aerial density and speed of the wave [1-3]. This particular effect is extremely difficult to capture in an experimental set up. Furthermore, the presence of rubber layer adjacent to ceramic having the highest stiffness among all components of the armor, makes the analysis very interesting.

It is apparent during ballistic event that the localized materials response in the vicinity of the applied load becomes primarily important whereas the overall geometric configuration of the structure becomes secondary. At the same time, due to the differences in the bending stiffness in a multi-materials armor system, the transmission of compression and rarefaction waves between the plates are significantly different than if it were only made from several layers of composites. In a typical composite system, the energy absorption mechanism during impact is the local deformation and fiber fracture. Delamination does not seem to have a major role in dissipating a large amount of energy. The idea however, contradicts significantly with the ballistic tests of integral armor. Delamination between the rubber and ceramic, or between the rubber and composites are found to be the major failure modes of the armor during impact. Of particular importance is the use of rubber with brittle ceramic. Analysis of the in- and out-of-plane stresses in these layers together with the determination of interlaminar stresses to study the structural integrity of the armor is the focus of this investigation.

Detailed description of the modeling approach and the discussion of the finite element and experimental results are presented in this paper.

Finite Element Modeling:

Several sets of finite element models have been developed to investigate the integral armor response to a penetrating bullet. In each model there are three main components namely ceramic, composite and rubber. These three material systems have been defined with three material types depending on their elastic properties. Material properties used in the finite element code are shown in Table-1. All material systems have been modeled with 8-noded solid elements. Material types and the number of elements along the thickness have been assigned in accordance with the actual construction of the layer. Ceramic, composites, and rubber are modeled with material type 13, 22 and 7 respectively. Material type 13 is an isotropic elastic-plastic element which allows application of failure criterion. The failure criterion in type 13 is based on the deviatoric components of the stress tensor and is controlled by user-defined parameters such as the minimum pressure and the maximum strain. The rubber layer has been modeled with hyperelastic continuum rubber element developed by Blatz and Ko [4]. The model utilizes the second Piola-Kirchoff stress theory as described in the reference [4]. On the other hand, for the composite layers of the integral armor, material model type 22 has been used. Three failure criterion, namely, matrix cracking, compression failure and fiber

breakage criterion have been used in this model. Detailed description of these failure modes can be found in the references [5,6].

The projectile has been modeled with material type 3 which contains formulations combining isotropic and kinematic hardening. Strain rate effect is accounted for by scaling the yield stress through a strain rate dependent factor [6].

The termination time for the finite element run was set at 150 μsec. After several iterations and after analyzing the maximum displacement and kinetic energy distributions of the bullet with respect to time, this particular value was arrived at. The displacement and KE of the bullet leveled off at around 110 μsec, and it was decided to run the program for 150 μsec. The time step used in the program was, $\Delta t = 0.01$ μsec which is also the default time step in DYNA3D.

Experiment:

High velocity impact tests on integral armor and on the components of the armor were carried out at the Tuskegee University's Center for Advanced Materials using a 76.2 mm (3") gas gun. The gas-gun barrel was 6.7m (22 ft) long and it was attached to a breech unit consisting of a pressure accumulator and the firing valve assembly. The actual impact took place in the experimental chamber which in turn was coupled to a recovery chamber to trap the projectile in case of complete penetration through the target. The gun was capable of launching a 14.0gm projectile with a velocity up to 610 m/s. The structural fragment simulated projectiles (FSP) shown in Fig.1 were used as penetrator. A sabot made from modulan 651 was used during the gas gun tests to carry the projectile. The projectile was released free after the sabot collapsed at a predetermined location prior to impact. The velocity of the projectile immediately before the impact was estimated using three equivalent magnetic sensors mounted at the gun nuzzle. After the tests, the damaged armors were photographed and C-scanned for damage analysis.

Results and Discussion:

The main objective of the finite element analysis was to investigate the response of the armor in the event of a projectile striking at a velocity close to V_{50}. It is understood that as far as ballistics are concerned, three layers, namely, ceramic, rubber and thick S2-glass, of the armor are most important. Analyses of their response in terms of stress and time are presented below.

After impact the kinetic energy of the projectile is imparted to the armor, and as the projectile penetrates the armor, the kinetic energy will be reduced while the internal energy of the system will increase. Distributions of these energies with respect to time are shown in Fig.2. Three energy distributions, namely, kinetic, internal and total energy distributions are shown in this figure. It is observed that the kinetic energy is reducing at a faster pace than the rate at which the internal energy is increasing. This causes the total energy to decrease moderately at the initial stage of the loading. The total energy distribution levels off at about 7.3×10^5 J around 40 μ sec and continues to stay at this magnitude through the remainder of penetration. Kinetic energy dissipation is an indication that the velocity of the projectile is being slowed down as it plows through the armor. The slowing down of the projectile can be visualized in Fig. 3. It is noticed that at around 110 μ sec the projectile has penetrated 21.6mm into the armor, and the z-displacement has begun to

level off suggesting that there is no displacement of the bullet with respect to time. This is a clear indication that the bullet has stopped. The displacement 21.6mm is the total rigid body displacement of the bullet from the initial time t = 0.0. If we add up the thicknesses from outside, i,e., from the signature layer, 21.6 mm suggests that the tip of the projectile has reached the end of the ceramic layer and it has been trapped there. However, from the experiments as seen in Fig. 4., the projectile in fact could not even penetrate to the middle of the ceramic layer, as most of the kinetic energy was consumed by the shattering of the ceramic tile. The failure of the FEM code to capture the experimental situation completely, is that the deviatoric components of stress and strain are set to zero when the failure strain is reached. Fracture in ceramics at very high strain rate will take place long before it reaches its quasi-static failure strain. In other words the failure criteria used in the model should be fracture based rather than strength based.

During impact, two stresses, namely, interlaminar tensile and interlaminar shear stress, are mostly responsible for causing damages to the armor. Since Z-direction has been set in the direction of the thickness, the interlaminar tensile/compressive stress in the present investigation is denoted by σ_z . This stress is perpendicular to the plane of the armor and can be tensile and compressive at different stages of time as the pressure pulse reverberates between the front and the back layers of the armor. It is obvious from the physical phenomenon of impact that distribution of σ_z will not only vary with respect to time but also across the thickness of the laminate and in the x-y plane of the armor. The finite element analysis has indicated that the location of the maximum σ_z for the whole armor is not at the tip of the bullet, rather it is very close to the periphery of the hole created by the projectile. The radial distance for this location is approximately 1.85mm from the periphery. The coordinates of the exact location of this point are; X=5.1, Y=10.7 and Z=27.2 mm. The Z coordinate of the point suggests that the overall maximum σ_z takes place in the ceramic layer. Figure 5 Shows the distributions of σ_z for three different layers; ceramic, rubber and S2-glass composites. It is observed that each layer has its own peak value of σ_z stress, ceramic being the largest. If we follow the propagation of σ_z stress in Fig. 5., it is seen that the time span for zero stress line is increasing as we move from ceramic to rubber and then to S2-glass layer. For the ceramic layer, the stress remains at zero level up to 10 μsec and then plunges to compressive stress of about 103 MPa before turning into tensile stress within the next 4-6 μsec. The time span for zero stress in the rubber layer is about 13 μsec, while it is around 28 for the composite layer. As the depth of the layers is increasing, it is taking longer and longer time for the stress pulse to get to those layers. For the phenolic layer on the back, it is taking about 30 μsec for the first pulse to arrive. If this pulse were to return as tensile wave and cause the tensile stress in the ceramic layer, that is not clearly happening. The pulse while returning should invariably take more than 4-6 μsec to get to the ceramic layer. The possible explanation for this instantaneous shift to tensile mode is that the pulse is partially reflected at the ceramic-rubber interface causing it to become tensile. We observe that the ceramic layer is experiencing the maximum σ_z stress, approximately 552 MPa. If the interface or the bonding between the rubber and ceramic is not strong enough to withstand this high surge of tensile wave, delamination failure will take place. The next level of tensile σ_z stress, approximately 172MPa is observed in the rubber layer, which will eventually pass on to the interface between the rubber and the S2-glass composites.

Therefore, it seems that this interface too is vulnerable to the tensile wave. Photograph from an actual gas gun test is shown in Fig. 4. The figure demonstrates that the failure of the armor is composed of two major failure modes; one is the crushing of the ceramic due to large σ_z in that layer, and the other is the complete delamination due to high interlaminar stresses. As seen in Fig. 4., both ceramic and S2-glass layers across the rubber layer have completely debonded supporting our previous analysis that these two interfaces are most important to be looked into during the fabrication of the armor panels. The general distributions of σ_z as seen in Fig. 5. for all the three layers are alternating in nature with respect to time as it is expected in an impact situation like this.

If we now look at the distribution of σ_z across the thickness of the armor at a particular instant of time ($t = 2.4x10^{-5}s$), it is observed that the largest tensile σ_z stress is at the ceramic layer as shown in Fig 6a. As one approaches towards the rubber layer, σ_z turns from tensile to compressive. Boundaries of each layer of the integral armor are also shown in Fig 6a. It is noticed that the two interfaces on both sides of the rubber layer are experiencing compressive σ_z . This suggests that at the particular time step, the interfaces should not delaminate due to σ_z . However, as the time step increases, for example at $t = 9.9x10^{-5}$ sec as shown in Fig 6b, the ceramic-rubber interface is seen to experience positive σ_z which is known as interlaminar tensile stress (ILT). On the other hand, the rubber-composite interface is still under compressive stress. If we further increase the time step, the compressive stress on this interface reduces and approaches to zero but never turns to tensile. What this implies is that the most vulnerable interface for delamination failure is the ceramic-rubber interface. In Fig. 4 we have observed that in fact both interfaces had failed during the experiment indicating that there are other interlaminar stresses responsible for the delamination of the rubber-composite interface. Besides σ_z the other interlaminar stresses are τ_{yz} and τ_{zx} . The finite element analysis has predicted very low values of τ_{zx} , however, the magnitudes of τ_{yz} as shown in Fig. 7 are considerably high. The τ_{yz} versus time plot of Fig. 7 is for a rubber element at the rubber-composite interface. It is observed that at around $t = 5.0x10^{-5}$ second, the τ_{yz} stress reaches as high as 8 MPa which is sufficient to cause delamination at that interface. In further assessment of the failure of the interfaces, the relative z-displacements between the nodes across each of the two interfaces are shown in Fig. 8. The maximum relative nodal displacements for the ceramic-rubber interface as seen in Fig. 8, is almost half of what is observed for the rubber-composite interface. The z-displacements shown in Fig. 8 is mainly due to the local bending of the armor, and it is clear that ceramic did not bend as much as the composite layer did. Because of the viscoelastic nature of rubber, it will not have any difficulty in deforming along with the ceramic prior to separation, but since the deformation of ceramic is much smaller than that of composite, the interface between rubber and composite will therefore, tend to open up.

So far we have discussed about interlaminar stresses, however, the stresses that will cause local bending and fiber fracture is the bending stress, σ_x. Global bending of the armor is expected to be negligible as the stiffness of ceramic is high and the bending stiffness is proportional to the cube of the thickness of the armor. In a local sense, the distribution of σ_x with respect to time for an element on the back surface of the armor is shown in Fig.9. Stress pulse takes about 30 μsec to reach the back surface and σ_x remains

tensile throughout the time domain as seen in Fig. 9. It is interesting to note that the bending stress keeps increasing as the time step increases. This suggests that as the bullet penetrates the armor from the front side, the bulging of the back face will continue to grow. This bulging will however, be very local surrounding the area of the projected path of the bullet. Contour plot of σ_x stress on the back face of the armor supports this fact. The distribution of σ_x through the thickness of the armor as shown in Fig. 10 indicates that the armor is somewhat under bending. Compressive σ_x in the front portion of the armor is understandable, but the large tensile stress being experienced by ceramic layer, and compressive stress in the rubber layer are not typical of pure bending. Transition from tensile to compressive or vice versa is taking place between the ceramic, rubber and thick composite laminates and their interfaces. This again points to the fact that the interfaces between these three layers are critical. The compressive σ_x stress as seen in Fig. 10 becomes tensile after it crosses the mid-thickness of the ceramic layer. As it approaches towards the rubber layer, σ_x turns compressive and again tends to become tensile as one moves to the back surface. However, even at the back face, the magnitude of the tensile stress is much lower than what is observed in the ceramic layer. This large σ_x, and considerably large σ_z seen before, all on the ceramic layer are responsible for the damages on the tiles as observed in Fig. 4.

SUMMARY:

The following conclusion can be drawn from the above discussion:

1. At V_{50} velocity, a 12.7 mm caliber FSP generates the maximum in-plane and transverse normal stresses in the ceramic layer of the armor. While the projectile is trapped by the ceramic layer, it causes substantial localized damage to the ceramic tile in the form of disintegrated powdered particles. The fracture pattern in ceramic allows faster dissipation of energy which helps arrest the projectile within the armor. The material model used in the FEM model is strength based which cannot fully capture the deformation scenario in ceramics. The material model may be modified on the basis of fracture.
2. Reflection of the stress wave at the ceramic-rubber interface causes instantaneous shift of the incoming compressive pulse to a tensile pulse. This makes this interface potentially vulnerable to delamination. Experimental studies have corroborated this finding.
3. The location of maximum transverse normal stress (σ_z) is not at the tip of the projectile rather it is very close to the periphery of the hole created by the projectile.
4. The rubber-composite interface also fails by delamination, however, the stress responsible for such delamination is believed to be interlaminar shear stress rather than the interlaminar tensile stress.
5. Bending stress distribution also suggests that the critical sections in the armor are the interfaces across the rubber layer. σ_x changes sign across these two interfaces. Despite its location somewhere near the mid-thickness of the armor, the ceramic layer still undergoes the largest in-plane stress σ_x, which combined with σ_z stress causes severe damage to the ceramic layer during penetration.

6. Finally, a finite element analysis of an integral armor under high velocity impact is presented which can be used to assess the in-plane, transverse, and interlaminar stresses for failure analysis.

Acknowledgments:

The authors would like to thank the Army Research Office (ARO) for support of this work through Grant No. DAAH04-95-1-0369.

References:

1. Seglates, S.B. and Zukas, J.A., “The effect of Mechanical interfaces on calculations of Plate Penetration,” *Recent Advances in Impact Dynamics of Engineering Structures*, AMD-Vol. 105, AD-Vol. 17, ASME 1989, pp. 39-45.
2. Johnson, W., Impact Strength of Materials, Edward Arnold , London, 1972.
3. Zukas, J. A., Impact Dynamics, Wiley Interscience, New York, 1982.
4. Blatz, P. J., and Ko, W. L., "Application of Finite Element Theory to the Deformation of Rubber Materials," *Trans. Soc. of Rheology* 6, 223 - 251 (1962).
5. Blatz, P. J., and Ko, W. L., "Application of Finite Element Theory to the Deformation of Rubber Materials," *Trans. Soc. of Rheology* 6, 223 - 251 (1962).
6. Hallquist, J., LS - DYNA3D Theoretical Manual, Livermore Software Technology Corporation, May, 1998.

Table 1: Material Properties Used in the FEM Analysis

	E (Gpa)	G (Gpa)	ν	ρ (kg/m^3)
S2 plane weave	E_1: 56.00 E_2: 56.00 E_3: 15.03	G_{12}: 25.05 G_{23}: 20.01 G_{31}: 20.01	ν_{12}: 0.27 ν_{23}: 0.3 ν_{31}: 0.3	2.53E3
Carbon	E_1: 9.59 E_2: 9.59 E_3: 2.14	G_{12}: 1.72 G_{23}: 1.72 G_{31}: 1.72	ν_{12}: 0.2 ν_{23}: 0.2 ν_{31}: 0.2	1.40E3
Ceramic (Al_3O_2)	270.34	110.83	0.22	3.49E3
Rubber (EPDM)	4.00	0.76	0.2	1.34E3
S2 glass Twill Weave (Vinyl ester)	E_1: 53.03 E_2: 50.00 E_3: 15.03	G_{12}: 20.01 G_{23}: 15.03 G_{31}: 15.03	ν_{12}: 0.27 ν_{23}: 0.3 ν_{31}: 0.3	2.53E3
Phenolic	25.03	9.66	0.3	1.40E3

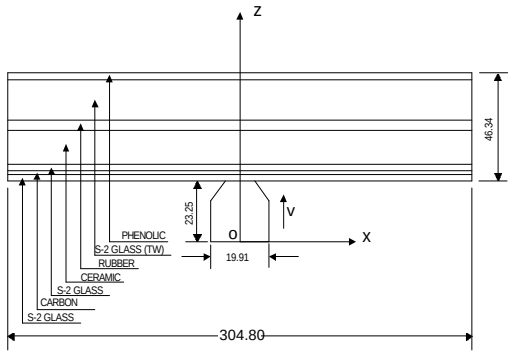

Fig. 1: A Schematic of the Fragment Simulated Projectile (FSP) and the Integral Armor

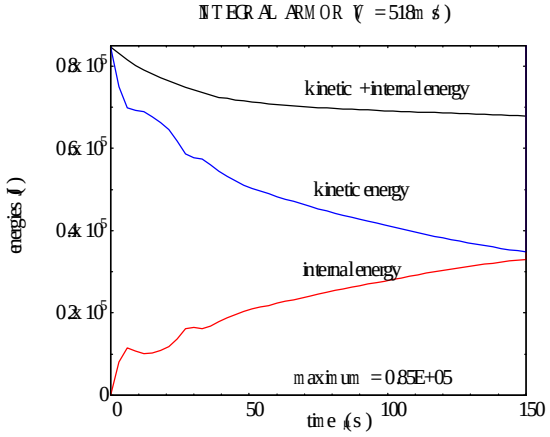

Fig .2: Energy of the Projectile vs Time

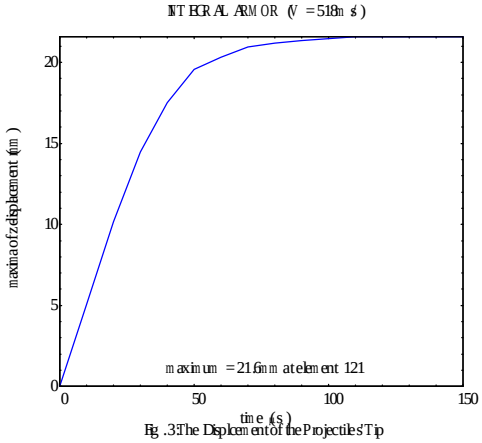

Fig .3: The Displacement of the Projectile's Tip

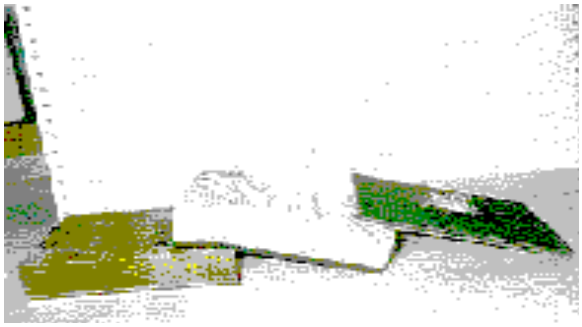

Fig. 4: Fractured Armor After Impact During a Gas Gun Test

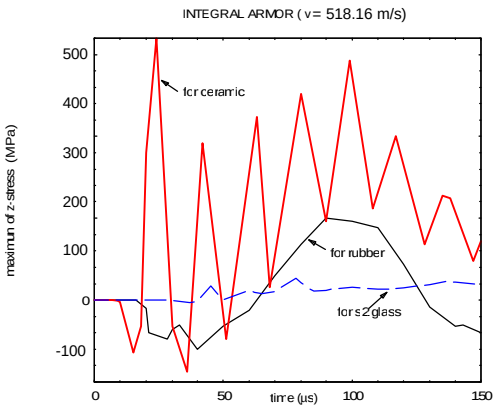

Fig. 5: Distribution of z-stress vs time

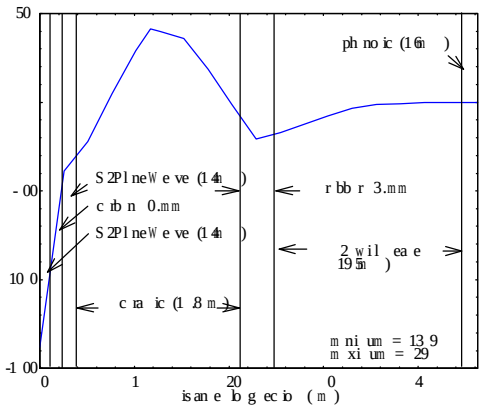

Fig. 6a: σ_z Distribution along Thickness (t = 24 μs)

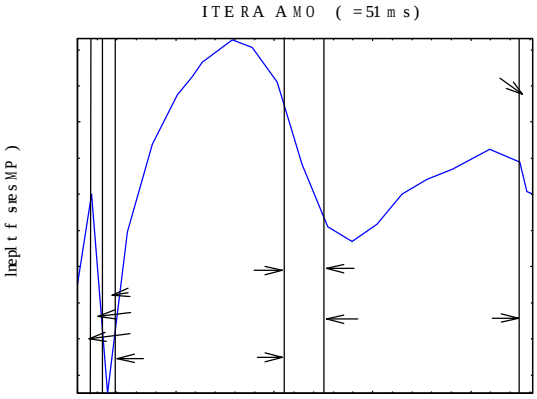

Fig. 6b: σ_z Distribution along Thickness (t = 99 μs)

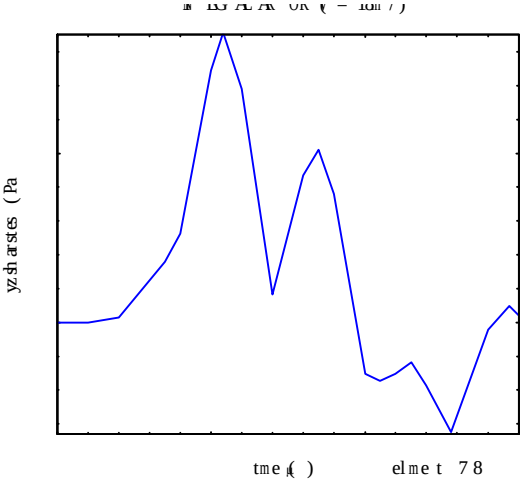

Fig. 7: τ_{yz} vs time at rubber-S2 glass interface

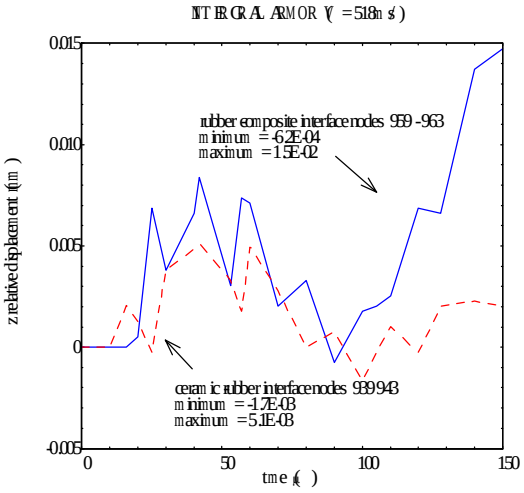

Fig. 8: The Relative Nodal Displacement

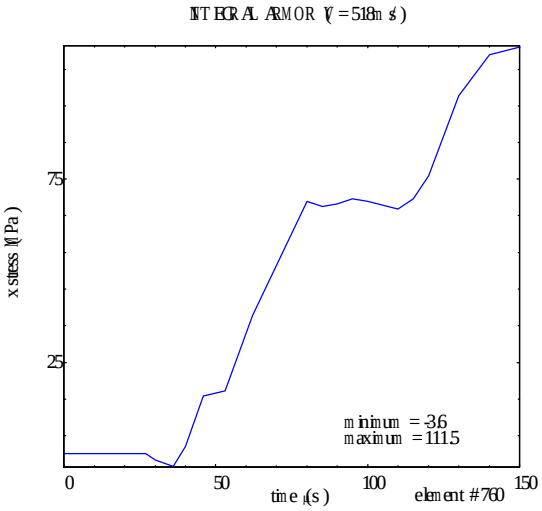

Fig. 9: σ_x vs Time at the Back Surface

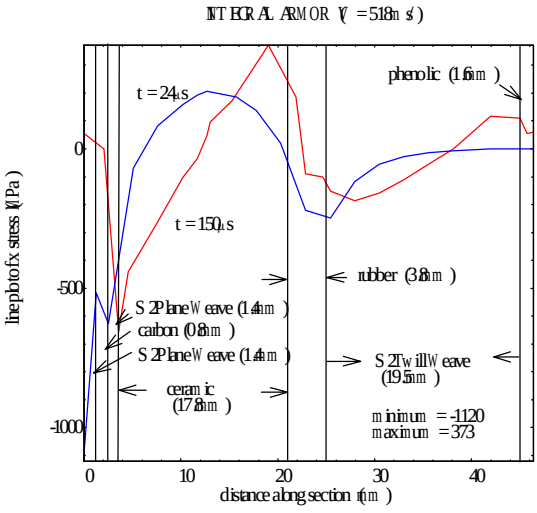

Fig. 10: σ_x Distribution along Thickness at Two Time Steps